

2D Materials



LETTER

RECEIVED
11 December 2016

REVISED
20 January 2017

ACCEPTED FOR PUBLICATION
8 February 2017

PUBLISHED
17 March 2017

The important role of water in growth of monolayer transition metal dichalcogenides

Christoph Kastl^{1,4}, Christopher T Chen^{1,4}, Tevye Kuykendall¹, Brian Shevitski^{1,2}, Thomas P Darlington^{1,2}, Nicholas J Borys¹, Andrey Krayev³, P James Schuck¹, Shaul Aloni¹ and Adam M Schwartzberg¹

¹ The Molecular Foundry, Lawrence Berkeley National Laboratory, Berkeley, CA 94720, United States of America

² Department of Physics, University of California, Berkeley, Berkeley, CA 94720, United States of America

³ AIST-NT, Novato, CA 94949, United States of America

⁴ Authors contributed equally.

E-mail: Saloni@lbl.gov and AMS@lbl.gov

Keywords: transition metal dichalcogenides, chemical vapor deposition, atomic layer deposition, vapor transport

Supplementary material for this article is available [online](#)

Abstract

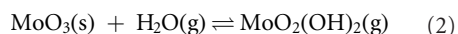
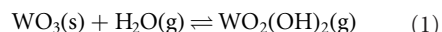
2D transition metal dichalcogenides (TMDs) are commonly grown by chemical vapor deposition using transition metal oxides as solid precursors. Despite the widespread use of this technique, challenges in reproducibility, coverage, and material quality are pervasive, suggestive of unknown and uncontrolled process parameters. In this communication, we demonstrate the impact of water vapor on this growth process. Our results show a direct correlation between gas phase water content and the morphology of TMD films. In particular, we show that the presence of water enhances volatilization, and therefore the vapor transport of tungsten and molybdenum oxide. Surprisingly, we find that water not only plays an important role in volatilization but is also compatible with TMD growth. In fact, carefully controlled humidity can consistently produce high quality, luminescent materials.

Interest in transition metal dichalcogenides (TMDs) has been renewed by the discovery of emergent properties when reduced to single, two-dimensional (2D) layers. The transition to direct band gap [1, 2], emerging charge density waves [3, 4], high mobility [5–7], and valley polarization [8–10] are some of the many exciting properties that have been reported in the TMD literature recently. A major bottleneck to this research is the lack of reproducible and large scale synthetic methods for high quality, consistent monolayer TMD samples. The dominant growth method is the vaporization and subsequent chalcogenization of solid metal oxides in the presence of gaseous chalcogen precursors. This process is commonly referred to as chemical vapor deposition (CVD) or powder vaporization [11–14]. Due to its simplicity, CVD is extensively used by the TMD community to produce high quality, micron-sized single crystals [11–13, 15–19]. Understanding the vaporization chemistry of solid transition metal precursors and vapor transport of volatilized precursors, particularly with respect to the influence of water vapor, is critical.

Humidity, i.e. water content of the reaction environment, is an important parameter in the gas phase

synthesis of inorganic materials, and while it is typically thought of as a contaminant, water is also an effective transport agent [20–23]. In this communication, we describe the synthesis of luminescent monolayer TMD islands by introducing water vapor as a simple means of controlling the volatilization and transport of the metal oxide precursor. Our experiments demonstrate a direct correlation between gas phase water content and the morphology of the resulting films. In particular, explicit control of the *in situ* water vapor concentration allows us to switch between two modes of growth: one in an effectively dry environment, in which the transition metal oxide source is converted directly to TMD material through a solid state reaction with the chalcogen source, and another in which the transition metal oxide undergoes vapor transport followed by reaction with the chalcogen source. We show that a small amount of water enhances the volatilization, and hence vapor transport, of the oxides of tungsten and molybdenum at the elevated temperatures (500–800 °C) used in the conversion or growth of their TMD counterparts. We attribute this effect to the enhanced vaporization of WO_3 and MoO_3 in the presence of water, first demonstrated in the 1930s and

1940s [24–27]. The well-established underlying mechanism is the formation of a volatile mono-hydroxide at elevated temperatures by a reversible reaction [21, 28]. In thermodynamic equilibrium the reaction reads



Achieving precise control of humidity at ppm levels in CVD reactors poses a significant challenge. First, water is a common contaminant of all commercially available process gases. Second, it is adsorbed on all exposed surfaces and is slowly released during growth. Lastly, the water content of air in a typical laboratory space is on the order of 10 000 ppm, which provides a constant source of available water vapor. In order to ensure a growth environment with precisely controlled humidity, the CVD furnace was regularly helium leak checked and purged with dry nitrogen outside of sample loading and CVD growth. After loading a sample and exposing the furnace to atmosphere, the furnace was pump-purged with ultra-high purity (99.999%) argon before initiating high temperature growth. With this level of control, we estimate that the baseline gas phase water concentration is ≤ 10 ppm. A schematic of the CVD reactor is shown in figure 1(a). Dry Argon is used as a carrier gas during growth and H_2S can be introduced as a chalcogenization agent when desired. The ratio between dry Ar carrier gas and Ar gas from a humidity reference with $c(\text{H}_2\text{O}) = 394$ ppm water can be adjusted to obtain the desired water concentration in the furnace.

Control of the chemical composition above the substrate is essential in isolating the factors governing nucleation and growth of thin films, as precursor delivery is especially critical in controlling the morphology of the reaction product. In this regard, solid precursors pose unique challenges—they typically have low volatility and low purity, and it can be challenging to control their evaporation kinetics due to surface and bulk contamination. These issues are further compounded by the high surface area inherent to the metal oxide powders commonly used for CVD. Therefore, in order to probe the effects of humidity on the vaporization of metal oxide precursors and subsequent growth of TMDs, it was necessary to use a source metal oxide that is finite and well quantified. We chose to use tungsten oxide films deposited by plasma assisted atomic layer deposition (ALD) as our source material. ALD has the benefit of consistently producing precise amounts of extremely flat materials with sub-angstrom thickness control. By using ultra-thin films it is clear when surface transport, vaporization, or conversion has taken place.

One of the major challenges in 2D film growth is controlling nucleation, a critical factor impacting domain size. Recent reports have shown that for CVD, TMD nucleation can be effectively controlled with conjugated organic molecules by simply spin-coating dilute solutions of these ‘seed’ molecules

onto the growth substrate [11, 29]. While the exact mechanism by which the seed molecules nucleate growth remains unclear, it is well documented that they increase crystal quality and allow control over the density of nucleation sites, enhancing reproducibility. Apparent nucleation sites seen in pristine [58] and PTAS-seeded [11] CVD growth of WS_2 and MoS_2 may be preferentially formed when the surface is functionalized with seed molecules [58]. For these reasons we tested the effect of seed molecules in water free and humid growth conditions. Perylene-3,4,9,10-tetracarboxylic acid tetrapotassium salt (PTAS) was chosen, as it is a widely used seed molecule system [11, 29].

Results and discussion

Using ALD deposited solid oxide precursors (1 nm in thickness, see Methods and Supporting information (stacks.iop.org/TDM/4/021024/mmedia)), we performed a systematic study with and without water vapor and PTAS seeding molecules. A schematic outline of our experimental approach is presented in figure 1(b). In the control experiment, metal oxide coated substrates were exposed to H_2S in a dry environment, resulting in the direct conversion from the oxide to a polycrystalline sulfide. When water vapor was introduced, the morphology of the surface was drastically changed to a mix of few-layer, multilayer, and wire-like structures. A second set of oxide substrates were spin-coated with PTAS seeding molecules to enhance nucleation. In dry conditions, crystalline TMD multilayer islands separated by bare silicon dioxide were formed. However, with the addition of 100 ppm of water, PTAS seeded substrates yielded crystalline TMD monolayer triangles.

Figure 2 shows scanning electron microscopy (SEM) images, atomic force microscopy (AFM) images, and Raman/photoluminescence (PL) spectra for each of the experimental conditions described. A detailed evaluation of the Raman spectra can be found in the supplementary information for each of the presented cases. Figure 2(a) shows a WO_3 film converted to WS_2 in a dry reactor. The conversion process of thin transition metal oxide films into transition metal dichalcogenide films has been previously demonstrated [30–34]. However, we note that our study also demonstrates that this direct, solid state conversion is only possible in the absence of moisture. The resulting film is composed of small, densely packed grains of WS_2 . This can be seen in the SEM and AFM images, which are effectively featureless, and in the Raman/PL spectrum, which clearly demonstrates the presence of WS_2 uniformly over the substrate. The low apparent PL intensity is likely due to the presence of small crystalline domains (~ 10 nm), where edge defects dominate the optical properties of the film. It should be noted that these films show a significant blue shift in their PL spectrum and in the in-plane vibrational modes compared to larger, single crystal monolayers. These observa-

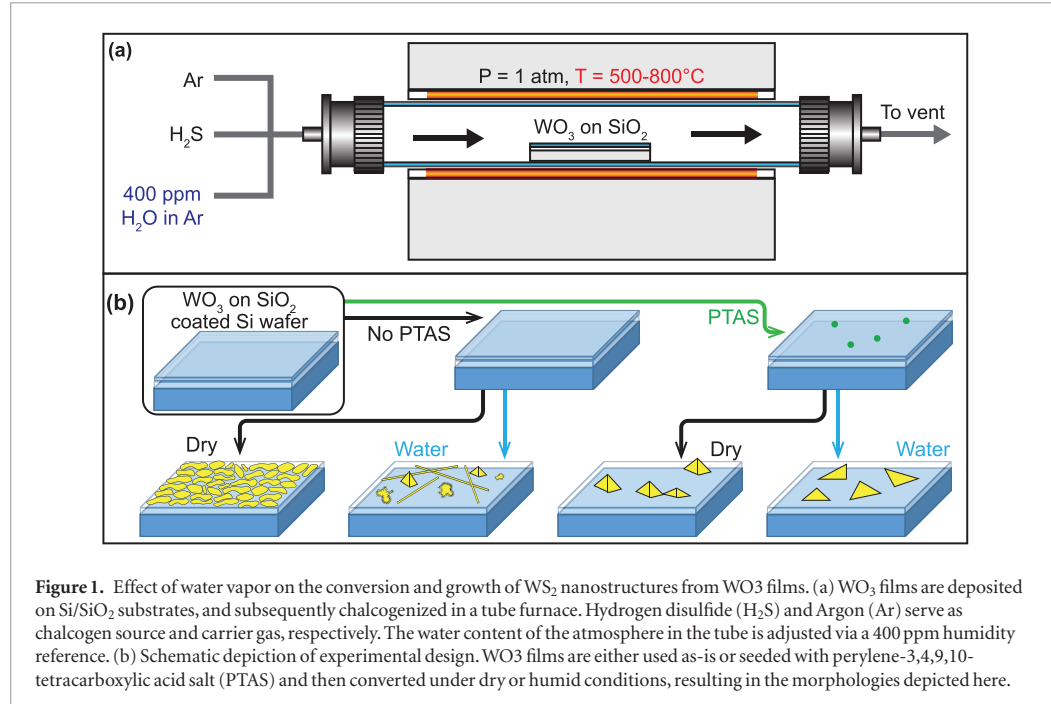


Figure 1. Effect of water vapor on the conversion and growth of WS_2 nanostructures from WO_3 films. (a) WO_3 films are deposited on Si/SiO_2 substrates, and subsequently chalcogenized in a tube furnace. Hydrogen disulfide (H_2S) and Argon (Ar) serve as chalcogen source and carrier gas, respectively. The water content of the atmosphere in the tube is adjusted via a 400 ppm humidity reference. (b) Schematic depiction of experimental design. WO_3 films are either used as-is or seeded with perylene-3,4,9,10-tetracarboxylic acid salt (PTAS) and then converted under dry or humid conditions, resulting in the morphologies depicted here.

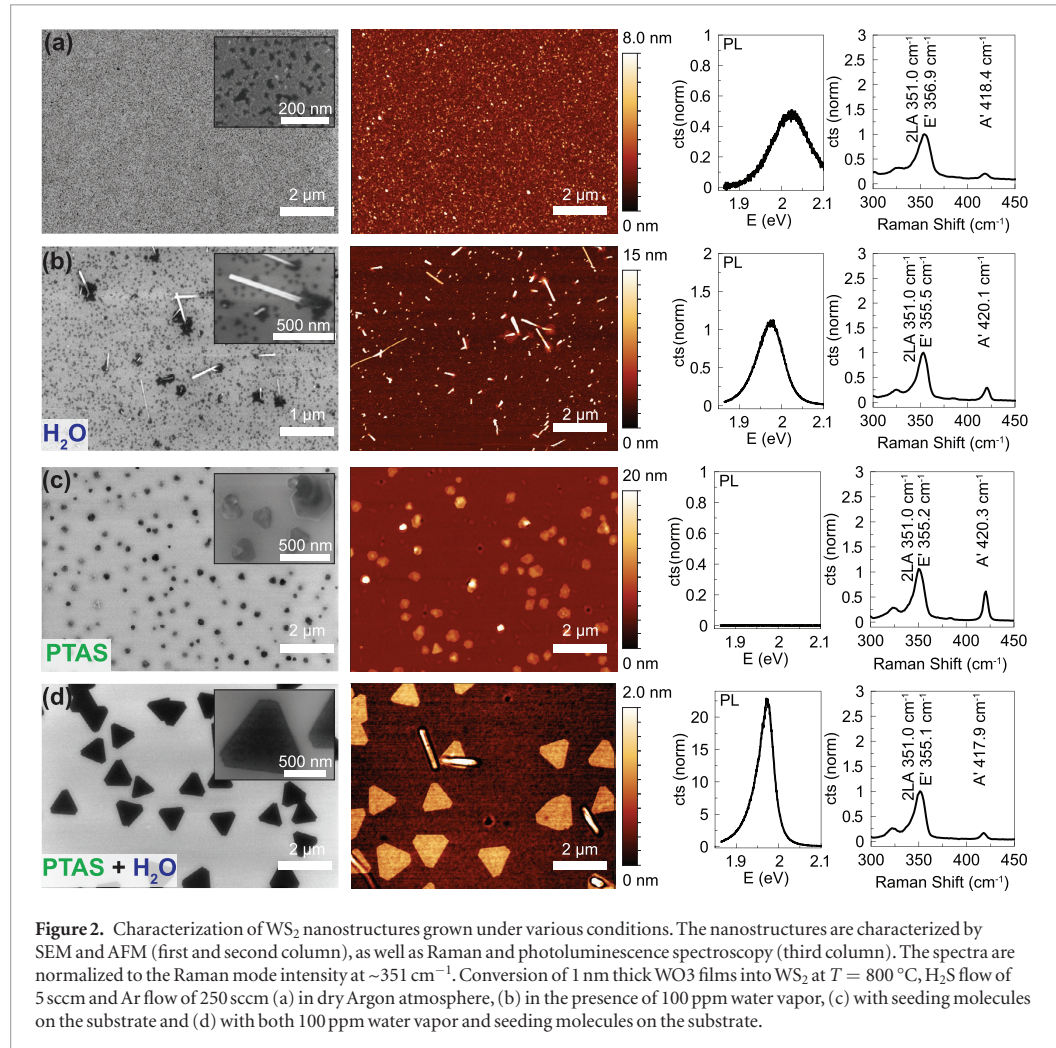
tions could be due to the presence of compressive strain in the polycrystalline films [35, 36].

As shown in figure 2(b), the addition of 100 ppm of water resulted in drastically modified film morphology compared to the water-free case. The SEM and AFM images are dominated by the presence of tube or wire-like structures, multi-layer patches, and some single layer regions of WS_2 . Further analysis with transmission electron microscopy (TEM) identifies some of the additional structures as WS_2 inorganic fullerenes and nanotubes in addition to the layered structure (supplementary information, figure S2). These additional phases were first observed in the conversion of W thin films to WS_2 and subsequently extensively studied by Tenne *et al* [41, 43, 59–61]. We hypothesize that the oxide after water-assisted volatilization has a morphology containing roughly spherical and elongated oxide structures, which are then converted into inorganic fullerenes [43] and nanotubes [61] respectively. Both Raman and PL reveal a combination of bulk material and monolayers. The monolayer regions show significantly increased PL and Raman intensity over the water-free case as well as an increased separation between the E_{2g}^1 and the A_g^1 mode of 65.5 cm^{-1} , likely due to the presence of few-layer domains. Large regions of the substrate do not show Raman nor PL signatures that are characteristic of WS_2 , suggesting that they are completely bare. From these observations it is clear that even small concentrations of water have a significant impact on the volatility and mobility of WO_3 during the growth process.

Figure 2(c) shows the result of the inclusion of PTAS during the dry conversion process. SEM and AFM imaging reveal bulk crystals over the entire surface, which were confirmed to be WS_2 by Raman spectr-

oscopy. The regions between the crystallites are bare, and no WS_2 or residual WO_3 was observed. Furthermore, the consistent shift of the out-of-plane vibrational mode by about $1\text{--}3\text{ cm}^{-1}$ and the lack of observable PL clearly preclude the existence of single- or bi-layer regions on the surface. Considering that under identical conditions, but without the seed molecules, the thin WO_3 films directly convert to WS_2 , it is apparent that the seed molecules nucleate crystals which then coarsen during the growth process.

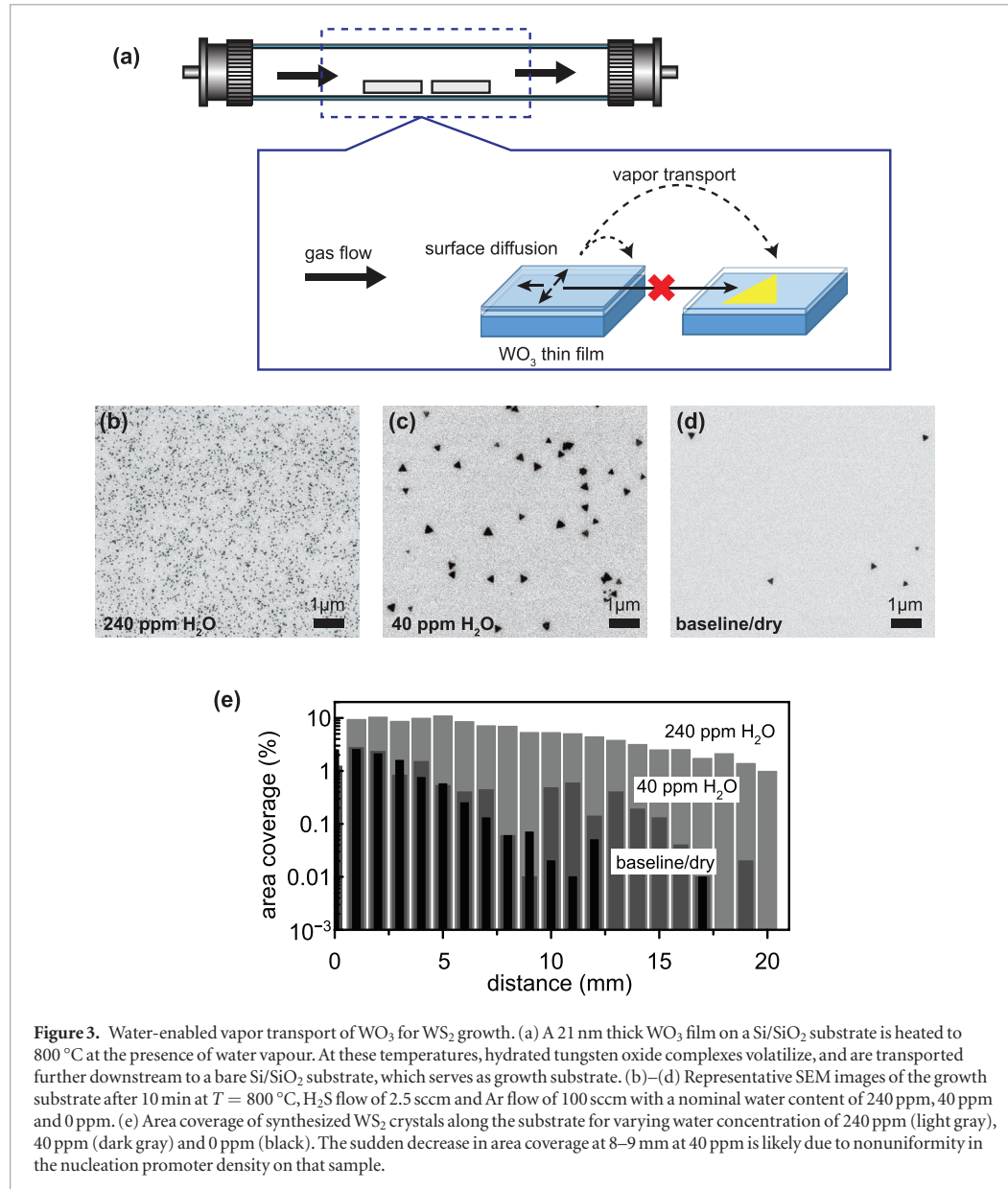
We now examine the effect of seeding molecules on the growth process in the presence of water. While we have already shown that water greatly increases the volatility of the WO_3 precursor and that seed molecules have a strong effect on the growth process, the combination of these two produce remarkable results, as shown in figure 2(d). With ~ 100 ppm of water vapor, micron-sized, monolayer single-crystalline islands form over the entire surface, as shown by SEM and AFM imaging. Across the growth substrate, the crystals showed uniformly intense PL, and the Raman spectra match those reported for monolayer WS_2 . The triangular islands are separated by bare SiO_2 , as confirmed by Raman spectroscopy. At intermediate water vapor concentrations, between the baseline and 100 ppm, the resulting morphology was an intermediate of the bulk crystalline and monolayer islands seen for dry and 100 ppm water seeded growth, respectively. At higher water vapor concentrations, the volatility of WO_3 was enhanced such that WS_2 could not be found after growth. It should be noted that water and oxygen have been reported to have significant effects on the photoluminescence intensity of MoS_2 and other monolayer TMDs when they are introduced after synthesis [37–39]. At ambient conditions, physisorbed water and oxygen reversibly dope 2D



TMDs. Depending on the prevalent type of charge carriers, the change in carrier density results in quenching or enhancement of the PL [37–39]. At elevated temperatures, water and oxygen can irreversibly create defects or oxidize the TMD [40]. In our study, trace amounts of water are introduced during the high temperature phase of the synthesis process. Generally, the reaction pathway from the metal trioxide MeO_3 to the metal sulfide MeS_2 can involve the release of water [41, 44]. This chemistry has been explicitly explored in the work of Weber *et al* for sulfurization of WO_3 and MoO_3 [62, 63]. Of note, they also found that while the reaction pathway for WO_3 and $\text{WO}_2(\text{OH})_2$ differ, the kinetics of sulfurization are quite similar for both cases [63].

Therefore, the addition of water does not open up any new reaction pathways. To limit the effect of oxidation on the resulting WS_2 , water vapor is introduced from the start of the heating process through only the first 5 min at the conversion temperature with H_2S , after which only Ar and H_2S gas are present in the input gas stream for the final 5 min of the conversion. As discussed later, the monolayers synthesized using water as a transport agent show optical properties which are comparable to previously reported TMDs grown via metal oxide powder-based CVD.

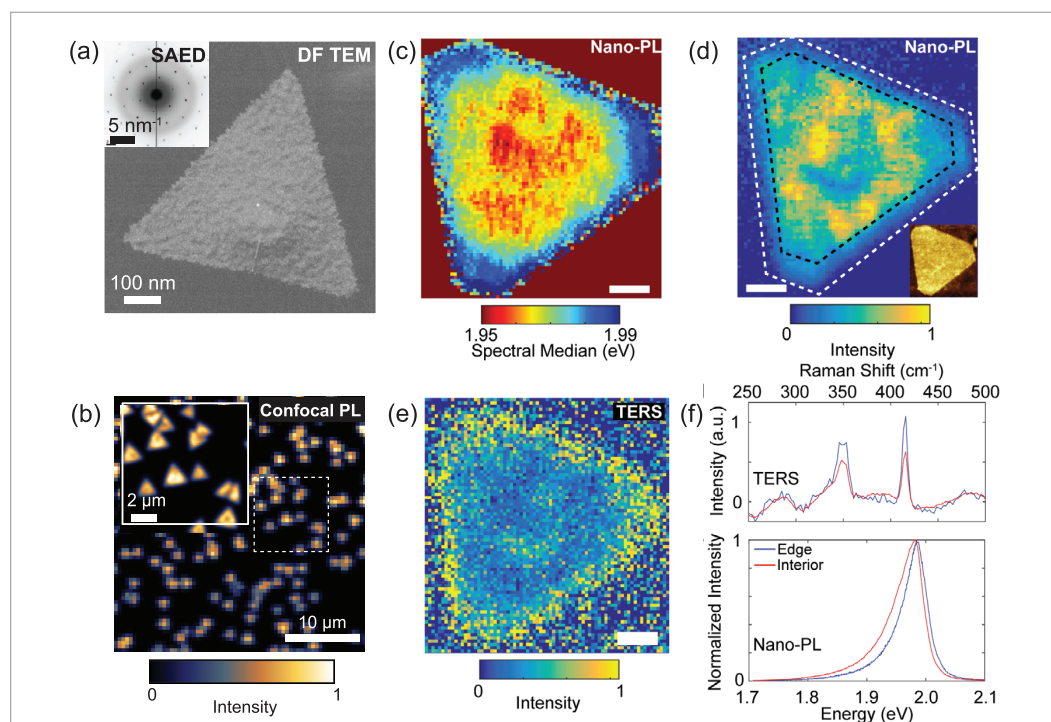
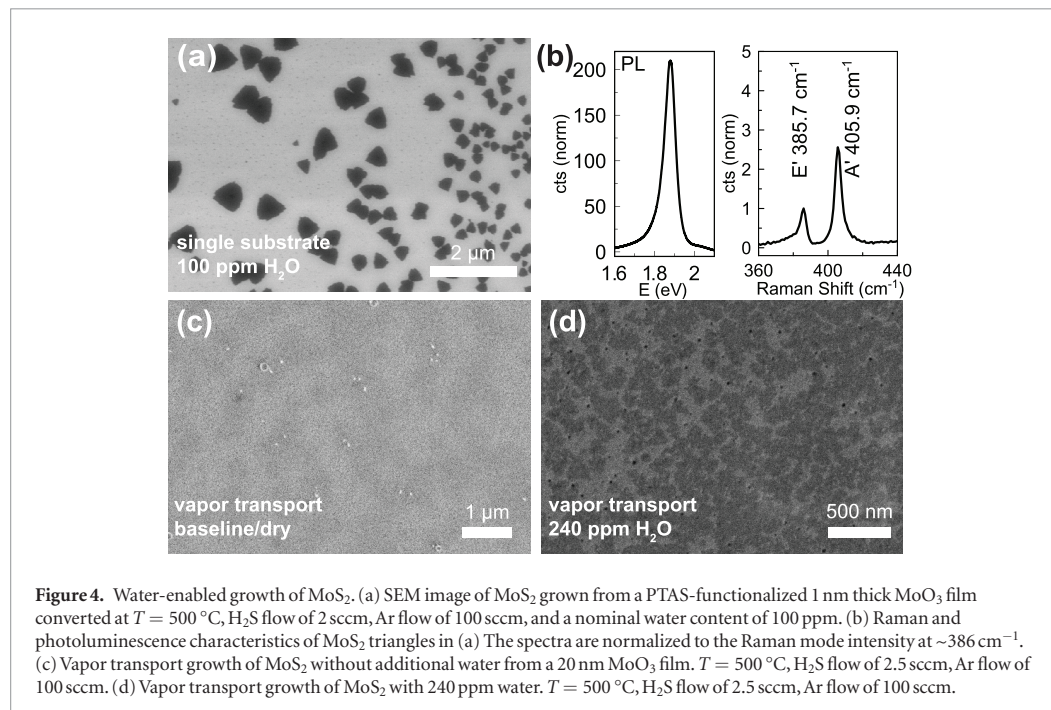
So far we have shown that water vapor modifies the growth process, and that WO_3 is significantly more mobile under these conditions. However, the prior experiments cannot distinguish between enhanced vapor transport and increased surface diffusivity. In the following, we show that the presence of water in the tube furnace primarily affected the volatilization and vapor transport of WO_3 . Si/SiO₂ substrates with 21 nm films of WO_3 were used as a vapor transport source, placed adjacent to a Si/SiO₂ substrate downstream, and the concentration of water vapor was varied at elevated temperature. Volatilized WO_3 was transported downstream to the growth substrate, whereupon it reacted with H_2S gas to form triangular WS_2 islands (figure 3(a)). To enhance nucleation, the growth substrates were pretreated with PTAS solution. Representative SEM images of the growth substrate are shown in figures 3(b), (c) and (d) for nominal water contents of 240 ppm, 40 ppm and 0 ppm, respectively. The images were recorded at the center of the substrates. We observe two distinct growth characteristics. First, the total area covered by WS_2 crystals increases with increasing water concentration. Figure 3(e) shows a systematic evaluation of the area covered by WS_2 as a function of position



on the growth substrate. The position starts from zero, where the two substrates abut, and increases towards the downstream edge. There is a clear trend of increased growth density and extent of vapor transport as the water concentration is increased. Second, the average size of the triangular islands decreases significantly for the highest water concentration. Generally, growth dynamics are governed by the competition between lateral growth of existing islands and nucleation of new sites [45]. As the reaction furnace is operated under sulfur rich conditions, the total growth rate of WS_2 is controlled mainly by the concentration of WO_3 precursor adsorbed on the substrate, which is proportional to the concentration of tungsten oxide in the gas phase [46]. Hence, we can assume that WS_2 growth on the surface approximately follows the concentration of WO_3 precursor in the gas phase. We attribute the correlation of total area coverage and water concentra-

tion to an enhanced growth rate due to the increased WO_3 concentration in the gas phase. At the same time, the increase of precursor in the gas phase leads to an increased nucleation rate. Therefore, the occurrence of small islands with high density at $c(\text{H}_2\text{O}) = 200$ ppm can be understood as a regime where the precursor is supplied in excess and the growth is limited by mobility of the reactants on the surface. For low water concentration ($c(\text{H}_2\text{O}) = 40$ ppm and baseline), the growth is limited by the precursor supply. Nucleation is largely suppressed and islands grow via surface diffusion of reactants, which results in much fewer but larger islands. Consequently, the data clearly show that the volatilization and extent of transport of tungsten oxide species is proportional and highly sensitive to the concentration of water vapor present in the furnace.

In order to demonstrate the generalizability of the effects of water on metal oxide vapor transport, we per-



formed identical studies with MoO_3 as the precursor film for the growth of MoS_2 . However, direct sublimation is particularly significant for MoO_3 , which has an equilibrium vapor pressure of 2.6 Torr at 750 °C [47], while it is less significant for the more stable WO_3 , which has a vapor pressure of 0.73 mTorr at 1041 °C [48]. Therefore, in order to demonstrate water assisted vapor transport, moderate temperatures with low MoO_3 vapor pressure were chosen; at higher temperatures, the formation of hydroxides competes with direct evaporation of the solid oxide into the gas phase [23]. Growth with a PTAS-seeded 1 nm MoO_3 thin film at 500 °C and 100 ppm water content produced MoS_2 monolayer crystals with bright photoluminescence as shown by the SEM image and PL spectrum in figures 4(a) and (b), respectively. While detailed studies of the extent of transport as a function of water concentration were not carried out, vapor transport experiments at 500 °C, with thick MoO_3 source wafers, showed little to no material deposition on the downstream substrate without additional water (figure 4(c)), and substantial MoS_2 growth with 240 ppm water (figure 4(d)). We note that, a quantitative relation between partial water pressure, temperature and partial oxide pressure was established by Glemser and Haeseler [28] under thermodynamic equilibrium conditions. The results can readily be applied to linear flow reactors if the total gas flow does not significantly disturb the equilibrium condition. For the apparent partial pressure of the metal oxide, which results from mono-hydroxide formation and direct sublimation, they find

$$P_{\text{oxide}} = K \cdot P_{\text{water}} + P_{\text{oxide}}^{(s)}$$

with partial water pressure P_{water} and partial oxide pressure $P_{\text{oxide}}^{(s)}$ from the direct sublimation of the metal oxide. The reaction constant K was experimentally determined as $\log K_{\text{Mo}} = -7731 K/T + 5.45$ for MoO_3 and $\log K_{\text{W}} = -8725 K/T + 4.10$ for WO_3 .

To further compare the WS_2 monolayer islands to other CVD-grown TMD materials, initial transmission electron microscopy, nano-photoluminescence (nano-PL) and tip-enhanced Raman scattering (TERS) characterization of monolayer- WS_2 crystallites were carried out (see experimental methods for details). Figure 5(a) shows a dark field image of a WS_2 monolayer that was directly grown by the water-assisted CVD on a SiO_2 coated Si_3N_4 -membrane. The inset selected area electron diffraction (SAED) pattern confirms the expected structure for a single crystal WS_2 layer. For the sample presented in figure 2(d), a scanning confocal PL image over a large area (figure 5(b)) shows relatively uniform emission over many small crystallites, and there are clearly resolution-limited features in each of the monolayer crystals (inset of figure 5(b)). Whereas the flakes are relatively uniform topographically, the intensity (figure 5(c)) and energy (figure 5(d)) of the excitonic PL exhibit pronounced nanoscale variations, including a distinct peripheral edge region (~110 nm wide)

of weaker PL and stronger TERS (figure 5(e)). Qualitatively similar nanoscale heterogeneity and peripheral edge regions have been previously reported for both CVD-grown monolayer- MoS_2 [49, 50] and WSe_2 [51] and are thought to arise from spatial variations in carrier density and crystalline disorder. The average TERS and nano-PL spectra of the interior and edge regions of our WS_2 are shown in figure 5(f). Compared to the interior, the A' vibrational mode is slightly enhanced with respect to the E' mode (figure 5(f)), while at the same time the PL narrows and is shifted to higher energy (figure 5(f)) within the edge region. Combined, these spectral signatures provide initial evidence that carrier density within the edge region is reduced, which is known to enhance the A' vibrational mode in monolayer- MoS_2 [52] and reduce the formation rate of lower-energy charged exciton states (i.e. trions), shifting the PL to higher energies [53, 54]. Although more detailed experimentation is needed to fully unravel the nanoscale photophysics in these samples, this initial nano-optical characterization reveals that these samples exhibit nanoscale optoelectronic heterogeneity that is remarkably similar to previously reported TMDs grown via metal oxide powder-based CVD.

Conclusion

In summary, we believe that part of the inconsistency and complexity seen in the TMD monolayer CVD literature can be traced to the unintentional presence (or absence) of water vapor during conversion/growth, which leads to insufficient control over the vapor transport of the metal oxide precursor. We have demonstrated that the presence of small amounts of water vapor plays an important role in the volatilization and transport of metal oxide precursor in 2D TMD growth. Carefully managing our precursor by using a thin oxide film, we showed that when using water vapor, it does not directly sulfidize, but instead reorganizes into a variety of structures on the surface. When seed molecules are deposited directly onto the oxide film, luminescent monolayer single-crystalline islands form. Understanding the role of humidity has allowed us to produce uniform, consistent, high quality, 2D WS_2 and MoS_2 islands through a CVD growth process. Introducing trace amounts of water into metal oxide based CVD constitutes a possibility to increase the volatilization of the metal oxide at a constant growth temperature, which is an important parameter for optimizing the growth conditions. Further, we speculate that use of water as a transport agent may not be limited to the oxides of W and Mo; oxides of V, Mn, Cr, Ni, Zr, and Sr are also candidates for water-assisted CVD growth [55].

Methods

ALD deposition of transition metal oxide precursor

As substrates, commercially available 250 nm thermal oxide on silicon was used. The substrates were

conformally coated with WO_3 or MoO_3 using plasma enhanced ALD deposition at $T = 40^\circ\text{C}$ – 200°C (details in SI). The surface roughness (rms) of the bare Si/SiO_2 (130 pm) and the ALD coated substrates (180 pm) was determined by AFM. We used bis(tert-butylimido)-bis-(dimethylamido) tungsten [56] and molybdenum hexacarbonyl [57] as precursors for WO_3 and MoO_3 , respectively, and oxygen plasma in an Oxford Instruments FlexAl ALD system. The ALD growth rate was calibrated using fixed angle *in situ* spectroscopic ellipsometry (*Woolam M-2000*).

Tube furnace/growth conditions

WO_3 (MoO_3) films deposited on Si/SiO_2 substrates were placed at the center of a 1 in. diameter tube furnace. Pure argon (*Praxair Ultra High Purity Grade, 99.999%*) passed through an oxygen/moisture trap -(*Agilent OT3-4*) served as a carrier gas. We used pure H_2S (*Praxair, 99.6%*) as the chalcogen source (<1 PPM water). After loading the samples, the tube furnace was pumped to low vacuum (~10 torr) and purged with dry Ar multiple times before restoring to atmospheric pressure under Ar flow. The ratio between nominally dry Ar carrier gas, and Ar gas with $c(\text{H}_2\text{O}) = 394$ ppm water, was adjusted to obtain the desired water concentration in the furnace. The center temperature of the furnace was increased from room temperature to the growth temperature ($T = 800^\circ\text{C}$ for WS_2 and $T = 500^\circ\text{C}$ for MoS_2) over 10 min and held at that temperature for 10 min in total. H_2S was added to the gas flow when the desired growth temperature was reached. For the experiments presented in figure 2, the H_2O supply was switched off after 5 min. Under these conditions, the temperature was maintained for an additional 5 min. For the experiments presented in figure 3, the H_2O supply was switched off after 10 min. In both cases after 10 min, the H_2S flow was set to zero, heating was switched off, and the furnace was purged with dry Ar gas (500 sccm) during cool down. Once the temperature in the hot zone fell below 400 °C, we switched to N_2 for purging. The process took place at atmospheric pressure. A 50 μMol -solution of Perylene-3,4,9,10-tetracarboxylic acid tetrapotassium salt (PTAS) in methanol and water was used as a seeding promoter.

Characterisation of TMD microstructures

Morphology and optical properties of the synthesized structures were characterized by atomic force microscopy (*Park NX-10*, tapping mode), electron microscopy (*Zeiss Ultra-55*, $E = 1$ keV–10 keV) as well as combined Raman and photoluminescence spectroscopy (*WITEC Alpha 300R* or *Horiba LabRAM Aramis*, $\lambda_{\text{excitation}} = 532$ nm). Elemental composition was verified by x-ray photoelectron spectroscopy (*Omicron Nanotechnology NanoAuger*). Transmission electron microscopy (*JEOL 2100-F 200 kV Field-Emission Analytical Transmission Electron Microscope*) was performed on electron-transparent 15 nm

thick Si_3N_4 windows in a Si frame prepared using conventional photolithography and etching techniques. To achieve a surface chemistry for the growth on Si_3N_4 membranes that is comparable to a thermal oxide coated Si substrate, the membranes were uniformly coated with 10 nm SiO_2 by ALD prior to growth. The nano-PL and TERS characterization were conducted on a near-field scanning optical microscope (*OmegaScope-R; AIST-NT*) coupled to a standard confocal Raman microscope and spectrometer (*XPlora; Horiba Scientific*) under ambient conditions at room temperature. A protected silver nanoscale tip (*Omni-TERS-FM*) was brought into contact with the sample and illuminated with 637 nm (for TERS) or 532 nm (for nano-PL) continuous wave laser excitation by an objective (100 \times , 0.7 NA) at an oblique angle of incidence of 65°. The same objective was used to collect emission from the sample which was then filtered and analyzed with the Raman spectrometer. The TERS and nano-PL imaging were performed in a specialized scanning mode (*DualScan; AIST-NT*) whereby emission was collected with the atomic-force feedback in both contact (5–20 nN) and semi-contact modes at each point in the scan. In semi-contact mode, near-field enhancement from the tip is negligible and the collected emission estimates the far-field background, which was subtracted from the emission that was acquired with the tip in contact mode to obtain the near-field components of the signal. The TERS spectra contained an additional photoluminescence background which was approximated with a bi-exponential fit and subtracted from the near-field spectra. Topography scans were made before, during and after the measurements to ensure the sample was not damaged. The approximate resolution of the TERS and nano-PL datasets is 20 nm.

Acknowledgments

Work at the Molecular Foundry was supported by the Office of Science, Office of Basic Energy Sciences, of the US Department of Energy under Contract No. DE-AC02-05CH11231.

References

- [1] Mak K F, Lee C, Hone J, Shan J and Heinz T F 2010 Atomically thin MoS_2 : a new direct-gap semiconductor *Phys. Rev. Lett.* **105** 136805
- [2] Lebegue S and Eriksson O 2009 Electronic structure of two-dimensional crystals from *ab initio* theory *Phys. Rev. B* **79** 115409
- [3] Neto A 2001 Charge density wave, superconductivity, and anomalous metallic behavior in 2D transition metal dichalcogenides *Phys. Rev. Lett.* **86** 4382–5
- [4] Barja S *et al* 2016 Charge density wave order in 1D mirror twin boundaries of single-layer MoSe_2 *Nat. Phys.* **12** 751–6
- [5] Podzorov V, Gershenson M E, Kloc C, Zeis R and Bucher E 2004 High-mobility field-effect transistors based on transition metal dichalcogenides *Appl. Phys. Lett.* **84** 3301–3
- [6] Zou X *et al* 2014 Interface engineering for high-performance top-gated MoS_2 field-effect transistors *Adv. Mater.* **26** 6255–61
- [7] Schmidt H *et al* 2014 Transport properties of monolayer MoS_2 grown by chemical vapor deposition *Nano Lett.* **14** 1909–13

- [8] Mak K F, He K, Shan J and Heinz T F 2012 Control of valley polarization in monolayer MoS₂ by optical helicity *Nat. Nanotechnol.* **7** 7494–8
- [9] Zeng H, Dai J, Yao W, Xiao D and Cui X 2012 Valley polarization in MoS₂ monolayers by optical pumping *Nat. Nanotechnol.* **7** 7490–3
- [10] Zhu B, Zeng H, Dai J and Cui X 2014 The study of spin-valley coupling in atomically thin group VI transition metal dichalcogenides *Adv. Mater.* **26** 5504–7
- [11] Lee Y-H *et al* 2012 Synthesis of large-area MoS₂ atomic layers with chemical vapor deposition *Adv. Mater.* **24** 2320–5
- [12] Liu H E, Wong S L and Chi D Z 2015 CVD Growth of MoS₂-based two-dimensional materials *Chem. Vapor Depos.* **21** 241–59
- [13] Kang K, Xie S, Huang L, Han Y, Huang P Y and Mak K F 2015 High-mobility three-atom-thick semiconducting films with wafer-scale homogeneity *Nature* **520** 656–60
- [14] Das S, Robinson J A, Dubey M, Terrones H and Terrones M 2015 Beyond graphene: progress in novel two-dimensional materials and van der Waals solids *Annu. Rev. Mater. Res.* **45** 1–27
- [15] Liu Z *et al* 2014 Strain and structure heterogeneity in MoS₂ atomic layers grown by chemical vapour deposition *Nat. Commun.* **5** 5246
- [16] Bao W *et al* 2015 Visualizing nanoscale excitonic relaxation properties of disordered edges and grain boundaries in monolayer molybdenum disulfide *Nat. Commun.* **6** 7993
- [17] Eichfeld S M *et al* 2015 Highly scalable, atomically thin WSe₂ grown via metal–organic chemical vapor deposition *ACS Nano* **9** 2080–7
- [18] Lee Y, Park S, Kim H, Han G H, Lee Y H and Kim J 2015 Characterization of the structural defects in CVD-grown monolayered MoS₂ using near-field photoluminescence imaging *Nanoscale* **7** 11909–14
- [19] Gong Y *et al* 2016 Synthesis of millimeter-scale transition metal dichalcogenides single crystals *Adv. Funct. Mater.* **22** 2009–15
- [20] Ritenour A J, Cramer R C, Levinrad S and Boettcher S W 2012 Efficient n-GaAs photoelectrodes grown by close-spaced vapor transport from a solid source *ACS Appl. Mater. Interfaces* **4** 69–73
- [21] Lenz M and Gruehn R 1997 Developments in measuring and calculating chemical vapor transport phenomena demonstrated on Cr, Mo, W, and their compounds *Chem. Rev.* **97** 2967–94
- [22] Koskiahde E, Cossement D, Paynter R, Dodelet J P, Jean A and Lombos B A 1989 Doping of GaAs epitaxial layers grown on (100) GaAs by close-spaced vapor transport *Can. J. Phys.* **67** 251–8
- [23] Schmidt P, Schmidt M, Binnewies M and Glau M 2013 *Chemical Vapor Transport Reactions-Methods, Materials, Modeling* (Rijeka: Intech) (<https://doi.org/10.5772/55547>)
- [24] van Nieuwenburg C J and Blumendaal H B 1931 The pneumatolytic synthesis of silicates, II *Recl. Trav. Chim. Pays Bas* **50** 989–96
- [25] Belton G R and McCarron R L 1964 The volatilization of tungsten in the presence of water vapor *J. Phys. Chem.* **68** 1852–6
- [26] Belton G R and Jordan A S 1965 The volatilization of molybdenum in the presence of water vapor *J. Phys. Chem.* **69** 2065–71
- [27] Millner T and Neugebauer J 1949 Volatility of the oxides of tungsten and molybdenum in the presence of water vapour *Nature* **163** 601–2
- [28] Glemser O and Haeseler R V 1962 Gasförmige hydroxide. IV. Über gasförmige hydroxide des molybdäns und wolframs Z. Anorg. Allg. Chem. **316** 168–81
- [29] Ling X, Lee Y-H, Lin Y, Fang W, Yu L, Dresselhaus M S and Kong J 2014 Role of the seeding promoter in MoS₂ growth by chemical vapor deposition *Nano Lett.* **14** 464–72
- [30] Lin Y-C, Zhang W, Huang J-K, Liu K-K, Lee Y-H, Liang C-T, Chu C-W and Li L-J 2012 Wafer-scale MoS₂ thin layers prepared by MoO₃ sulfurization *Nanoscale* **4** 6637
- [31] Elías A L *et al* 2013 Controlled synthesis and transfer of large-Area WS₂ sheets: from single layer to few layers *ACS Nano* **7** 5235–42
- [32] Song J-G *et al* 2013 Layer-controlled, wafer-scale, and conformal synthesis of tungsten disulfide nanosheets using atomic layer deposition *ACS Nano* **7** 11333–40
- [33] Kong D, Wang H, Cha J, Pasta M, Koski K J, Yao J and Cui Y 2013 Synthesis of MoS₂ and MoSe₂ films with vertically aligned layers *Nano Lett.* **13** 1341–7
- [34] Song J-G *et al* 2015 Controllable synthesis of molybdenum tungsten disulfide alloy for vertically composition-controlled multilayer *Nat. Commun.* **6** 7817
- [35] Wang Y, Cong C, Qiu C and Yu T 2013 Raman spectroscopy study of lattice vibration and crystallographic orientation of monolayer MoS₂ under uniaxial strain *Small* **9** 2857–61
- [36] Conley H J, Wang B, Ziegler J I, Haglund R F Jr, Pantelides S T and Bolotin K I 2013 Bandgap engineering of strained monolayer and bilayer MoS₂ *Nano Lett.* **13** 3626–30
- [37] Tongay S, Zhou J, Ataca C, Liu J, Kang J S, Matthews T S, You L, Li J, Grossman J C and Wu J 2013 Broad-range modulation of light emission in two-dimensional semiconductors by molecular physisorption gating *Nano Lett.* **13** 2831–6
- [38] Nan H, Wang Z, Wang W, Liang Z, Lu Y, Chen Q, He D, Tan P, Miao F, Wang X, Wang J and Ni Z 2014 Strong photoluminescence enhancement of MoS(2) through defect engineering and oxygen bonding *ACS Nano* **8** 5738–45
- [39] Varghese J O, Agbo P, Sutherland A M, Brar V W, Rossman G R, Gray H B and Heath J R 2015 The influence of water on the optical properties of single-layer molybdenum disulfide *Adv. Mater.* **27** 2734–40
- [40] Rong Y, He K, Pacios M, Robertson A W, Bhaskaran H and Warner J H 2015 Controlled preferential oxidation of grain boundaries in monolayer tungsten disulfide for direct optical imaging *ACS Nano* **9** 3695–703
- [41] Feldman Y, Frey G L, Homyonfer M, Lyakhovitskaya V, Margulis L, Cohen H, Hodes G, Hutchison J L and Tenne R 1996 Bulk synthesis of inorganic fullerene-like MS₂ (M = Mo, W) from the respective trioxides and the reaction mechanism *J. Am. Chem. Soc.* **118** 5362–7
- [42] Tsirlina T, Feldman Y, Homyonfer M, Sloan J, Hutchison J L and Tenne R 1998 Synthesis and characterization of inorganic fullerene-like WSe₂ material *Fullerene Sci. Technol.* **6** 157–65
- [43] Feldman Y, Lyakhovitskaya V and Tenne R 1998 Kinetics of nested inorganic fullerene-like nanoparticle formation *J. Am. Chem. Soc.* **120** 4176–83
- [44] Zak A, Feldman Y, Alperovich V, Rosentsveig R and Tenne R 2000 Growth mechanism of MoS₂ fullerene-like nanoparticles by gas-phase synthesis *J. Am. Chem. Soc.* **122** 11108–16
- [45] Venables J A, Spiller G and Hanbucken M 1984 Nucleation and growth of thin films *Rep. Prog. Phys.* **47** 399
- [46] Govind Rajan A, Warner J H, Blankenstein D and Strano M S 2016 Generalized mechanistic model for the chemical vapor deposition of 2D transition metal dichalcogenide monolayers *ACS Nano* **10** 4330–44
- [47] Fourcaudot G, Gourmal M and Mercier J 1979 Vapor phase transport and crystal growth of molybdenum trioxide and molybdenum ditelluride *J. Cryst. Growth* **46** 132–5
- [48] Blackburn P E, Hoch M and Johnston H L 1958 The vaporization of molybdenum and tungsten oxides *J. Phys. Chem.* **62** 769–73
- [49] Bao W *et al* 2012 Mapping local charge recombination heterogeneity by multidimensional nanospectroscopic imaging *Science* **338** 1317–21
- [50] Ogletree D F *et al* 2015 Revealing optical properties of reduced-dimensionality materials at relevant length scales *Adv. Mater.* **27** 5693–719
- [51] Park K-D, Khatib O, Kravtsov V, Clark G, Xu X and Raschke M B 2016 Hybrid tip-enhanced nanospectroscopy and nanoimaging of monolayer WSe₂ with local strain control *Nano Lett.* **16** 2621–7
- [52] Chakraborty B, Bera A, Muthu D, Bhowmick S, Waghmare U V and Sood A K 2012 Symmetry-dependent phonon renormalization in monolayer MoS₂ transistor *Phys. Rev. B* **85** 161403

- [53] Shang J, Shen X, Cong C, Peimyoo N, Cao B, Eginligil M and Yu T 2015 Observation of excitonic fine structure in a 2D transition-metal dichalcogenide semiconductor *ACS Nano* **9** 647–55
- [54] Mak K F, He K, Lee C, Lee G H, Hone J, Heinz T F and Shan J 2013 Tightly bound trions in monolayer MoS₂ *Nat. Mater.* **12** 207–11
- [55] Meschter P J, Opila E J and Jacobson N S 2013 Water vapor-mediated volatilization of high-temperature materials *Annu. Rev. Mater. Res.* **43** 559–88
- [56] Becker J S, Suh S, Wang S and Gordon R G 2003 Highly conformal thin films of tungsten nitride prepared by atomic layer deposition from a novel precursor *Chem. Mater.* **15** 2969–76
- [57] Diskus M, Nilsen O and Fjellvåg H 2011 Growth of thin films of molybdenum oxide by atomic layer deposition *J. Mater. Chem.* **21** 705–10
- [58] Cain J D, Shi F, Wu J and Dravid V P 2016 Growth mechanism of transition metal dichalcogenide monolayers: the role of self-seeding fullerene nuclei *ACS Nano* **10** 5440–5
- [59] Feldman Y, Wasserman E, Srolovitz D J and Tenne R 1995 High-rate, gas-phase growth of MoS₂ nested inorganic fullerenes and nanotubes *Science* **267** 222–5
- [60] Margulis L, Salitra G, Tenne R and Talianker M 1993 Nested fullerene-like structures *Nature* **365** 113–4
- [61] Rothschild A, Sloan J and Tenne R 2000 Growth of WS₂ nanotubes phases *J. Am. Chem. Soc.* **122** 5169–79
- [62] van der Vlies A J, Prins R and Weber T 2002 Chemical principles of the sulfidation of tungsten oxides *J. Phys. Chem. B* **106** 9277–85
- [63] van der Vlies A J, Kishan G, Niemantsverdriet J W, Prins R and Weber T 2002 Basic reaction steps in the sulfidation of crystalline tungsten oxides *J. Phys. Chem. B* **106** 3449–57